Revista Mexicana de Astronomía y Astrofísica, **47**, 159–171 (2011)

TEMPERATURE, BRIGHTNESS AND SPECTRAL INDEX OF THE CYGNUS RADIO LOOP

V. Borka Jovanović[1] and D. Urošević[2]

Received 2010 October 18; accepted 2011 February 10

RESUMEN

Se presenta el brillo estimado del remanente de supernova del Velo del Cisne en 2720, 1420, 820, 408 y 34.5 MHz. Mediante el método que hemos desarrollado anteriormente para anillos grandes, utilizamos las observaciones de radioemisión en el continuo para calcular las temperaturas de brillo medias y los brillos superficiales del Velo del Cisne en las frecuencias mencionadas. Estimamos el espectro de las temperaturas medias versus frecuencia entre las cinco frecuencias y obtenemos el índice espectral del Velo del Cisne. Nuestros resultados muestran que el Velo evoluciona en un medio de baja densidad, y que la energía inicial de la explosión de supernova fue relativamente baja. Confirmamos el origen no-térmico de la radiación del anillo del Cisne y mostramos que nuestro método es aplicable a la mayoría de los remanentes de supernova.

ABSTRACT

The estimated brightness of the Cygnus loop supernova remnant (SNR) at 2720, 1420, 820, 408 and 34.5 MHz is presented. The observations of the continuum radio emission are used to calculate the mean brightness temperatures and surface brightnesses of this loop at the five frequencies in a wide spectral range, using the method we have previously developed for large radio loops. The spectrum for mean temperatures versus frequency between the five frequencies is estimated and the spectral index of the Cygnus loop is obtained. Also, from our results it can be concluded that the Cygnus loop evolves in a low density environment and that the initial energy of the supernova explosion was relatively low. The results obtained confirm the non-thermal origin of the Cygnus radio loop and show that our method is applicable to almost all remnants.

Key Words: ISM: supernova remnants — radiation mechanisms: non-thermal — radio continuum: general — surveys

1. INTRODUCTION

In our investigation, we are supposing the radio loops to be evolved supernova remnants (SNRs). Supernova remnants represent shells of approximately spherical shape which are spreading, and depending of the interstellar matter density, they change their shape. We can see only parts of these spherical contours which represent radio spurs, i.e., areas of more intense emission in the sky, spur-like and of huge dimensions. Radio loops consist of several spurs lying approximately on the same small circle of the celestial sphere. Their material probably expands inside of bubbles of low density. Bubbles are made by former SNR explosions or by strong stellar winds (Salter 1983; McKee & Ostriker 1977, and references therein). The radio emission from SNRs is generally understood to be synchrotron emission from relativistic electrons moving in the magnetic field.

A star in the constellation of Cygnus exploded and its remnant is the Cygnus loop. It is classified as a mid-aged SNR of type S, is located below (but near the plane of) the Galactic equator, and is less than 1 kpc away from us. It is listed in Green's catalogue of SNRs as G74.0-8.5 (Green 2004, 2006, 2009). As shown in Green (1984), this remnant has decelerated considerably by its interaction with the surrounding interstellar medium.

[1]Vinča Institute of Nuclear Sciences, University of Belgrade, Serbia.
[2]Faculty of Mathematics, University of Belgrade, Serbia.

Leahy, Roger, & Ballantyne (1997) presented high resolution 1420 MHz total intensity and polarization maps of the Cygnus loop and derived rotation measures. Aschenbach & Leahy (1999) made a comparison between the radio and X-ray emission from supernova remnants. The X-ray emission traces the hot gas behind the shock front, while the radio emission comes from the relativistic electron population emitting synchrotron radiation in the ambient magnetic field. They found that there are significant differences in the distribution of X-ray and radio brightness in the Cygnus loop. Also, significant temperature variations, seen along the rim and in the bright filaments interior to the rim, indicated that the Cygnus loop was caused by a supernova exploding in a cavity.

Uyaniker et al. (2002) suggested that the Cygnus loop may consist of two overlapping remnants. Substantial differences between the northern and southern part as well as in their emission characteristics have been observed (Uyaniker et al. 2004; Patnaude et al. 2002). Some authors proposed that the Cygnus loop consists of two likely interacting SNRs: G74.3-8.4 and G72.9-9.0 (Uyaniker et al. 2002; Leahy 2002). In Sun et al. (2006), from 4800 MHz observations, it is explained that the polarization maps (the difference in the polarization characteristic between the northern and southern part) support previous ideas that the Cygnus loop may consist of two SNRs. Besides, several compact radio sources are located within the boundary of the remnant. The main characteristics of the Cygnus loop in different spectral bands are: (a) in the radio band it is shell, brightest to the north-east, with fainter breakout regions to the south, with spectral variations; (b) in the optical it is a large filamentary loop, brightest to the north-east, not well defined to the south and west; (c) it is a shell in soft X-rays (see e.g., Green 2006).

Some radio maps which include this remnant are the following: the map by Kundu & Becker (1972) at 4940 MHz, Keen et al. (1973) at 2695 MHz, Uyaniker et al. (2004) at 2675 MHz, Leahy et al. (1997) at 1420 MHz, Dickel & Willis (1980) at 610 MHz, Green (1984) at 408 MHz. We found observations of the continuum radio emission at 2720 MHz (Reif et al. 1987), 1420 MHz (Reich & Reich 1986), 820 MHz (Berkhuijsen 1972), 408 MHz (Haslam et al. 1982) and 34.5 MHz (Dwarakanath & Udaya Shankar 1990), in electronic form and used them in this paper.

In our previous paper (Borka Jovanović & Urošević 2009a) we only calculated the temperatures and brightnesses at three frequencies. In this paper we expand the scope of our investigation to: brightness temperatures and surface brightnesses at five frequencies, as well as spectrum, $T-T$ graphs, radio spectral indices, an estimation of environment density and the initial energy of supernova explosion, and the flux density spectrum.

In our calculations, we used brightness temperatures over the whole area of the loop, so the mean temperature we estimated refers to the northern and southern parts together. In this research the average brightness temperatures and surface brightnesses of the Cygnus radio loop are calculated at the five frequencies: 2720, 1420, 820, 408 and 34.5 MHz. Then we study how these results compare with previous results (Roger et al. 1999; Reich, Zhang, & Fürst 2003; Uyaniker et al. 2004) and with current theories of SNR evolution. These theories predict that loops are non-thermal sources which are spreading inside the hot, low density bubbles made by former supernova explosions or by strong stellar winds (see Salter 1983; McKee & Ostriker 1977, and references therein).

Our aim is also to apply the method for the determination of the brightness temperature given in Borka (2007) which was developed for large radio loops, and to show that it is rather efficient in the case of much smaller radio loops, e.g., the Cygnus loop. We also check whether the results obtained using this method agree with the method of $T-T$ graphs and with results obtained with other methods. Our method is quite simple because we are using brightness temperature isolines to define borders of the Cygnus loop at the wide range of frequencies ($\nu_{\rm max}/\nu_{\rm min} = 2720\,{\rm MHz}/34.5\,{\rm MHz} \approx 79$). Other authors use different square or rectangular areas to determine the area of the loop and to calculate spectral indices, the brightness temperature and the flux of the loop (Uyaniker et al. 2004, page 917, and Leahy & Roger 1998, page 786). Also, we calculate the flux from the Cygnus loop and compare our results with results of other authors in different frequency ranges.

2. ANALYSIS

2.1. *Data*

We used the following radio-continuum surveys as the basic source of data in this paper: at 2720 MHz (Reif et al. 1987), 1420 MHz (Reich & Reich 1986), 820 MHz (Berkhuijsen 1972), 408 MHz (Haslam et al. 1982) and 34.5 MHz (Dwarakanath & Udaya Shankar 1990). These surveys are available in electronic form, in Flexible Image Transport System (FITS) data format[3]. This online survey sampler of the *Max-Planck-Institut für Radioastronomie* (MPIfR) near Bonn, Germany, allows users to pick a region of the sky and obtain images and data at different frequencies. The 2720-MHz Stockert survey has an angular resolution of 0°.35, the 1420-MHz Stockert survey (Reich & Reich 1986) 0°.59, the 820-MHz Dwingeloo survey (Berkhuijsen 1972) 1°.2, the 408-MHz all-sky survey (Haslam et al. 1982) 0°.85, and the 34.5-MHz Gauribidanur survey (Dwarakanath & Udaya Shankar 1990) 0°.7. The corresponding observations are given at the following rates (measured data) for both l and b: 1°/8 at 2720 MHz, 1°/4 at 1420 MHz, 1°/2 at 820 MHz, 1°/3 at 408 MHz and 1°/5 at 34.5 MHz. The effective sensitivities are about 5 mK T_b (T_b is an average brightness temperature), 50 mK, 0.20 K, 1.0 K and about 700 K, respectively.

FITS data format stores the multidimensional arrays and 2-dimensional tables containing rows and columns of scientific data sets. We extracted observed brightness temperatures from this data format into ASCII data files, and afterwards, using our programs in C and FORTRAN, we obtained the results presented in this paper.

2.2. *Method*

As there is a great influence of background radiation over the Cygnus loop area, it is very difficult to determine its area precisely. The area of this loop is enclosed with brightness temperature contours. The maps of a region in Cygnus, in new Galactic coordinates (l, b), with contours of the brightness temperatures T_b are plotted in Figures 1–5. In these figures, among all the brightness temperature contours, the most important are the outer contour and inner one, which represent the loop borders. The outer one (which corresponds to the minimum temperature of the loop) separates loop and background, while the inner one (corresponding to the maximum temperature) separates the loop and some superposed source. The interval of Galactic longitude of this loop is l=[76.5°, 71.5°], and of latitude it is b=[−10.5°, −7°]. We used the same method of calculation as given in Borka (2007) for Galactic radio loops I–VI, Borka, Milogradov-Turin, & Urošević (2008) for Loops V and VI and in Borka Jovanović & Urošević 2009b for the Monoceros loop. Our aim is to apply our method, which we developed for main Galactic loops I-VI and described in Borka (2007) and Borka et al. (2008), to smaller remnants and to

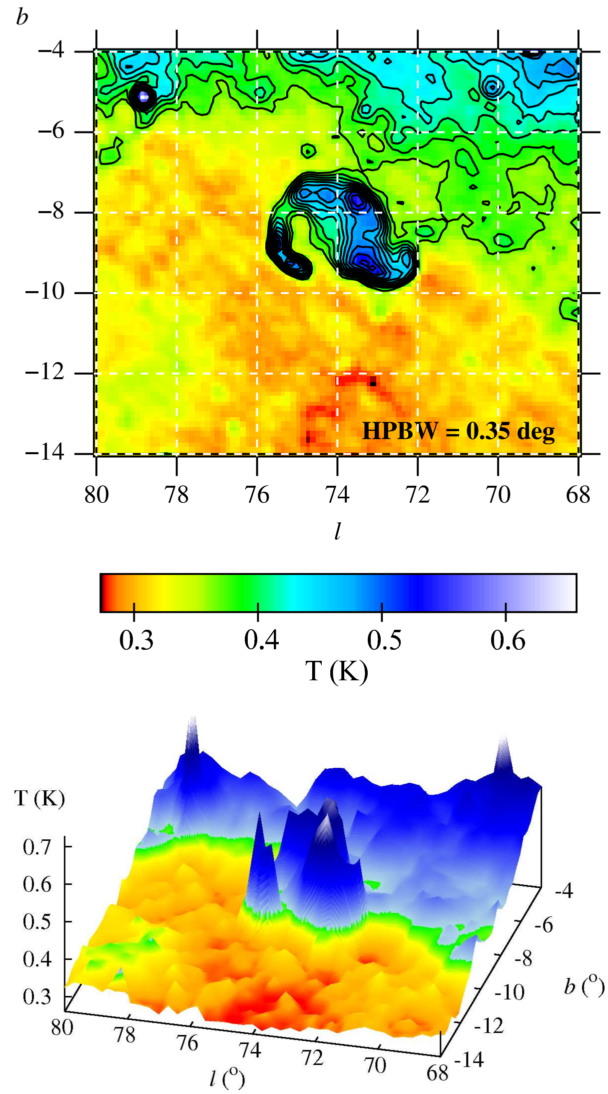

Fig. 1. Top: the 2720 MHz map of a region in Cygnus, in new Galactic coordinates (l, b), showing contours of brightness temperature. This radio loop has position: $l = [76.5°,\ 71.5°]$; $b = [-10.5°,\ -7°]$. The HPBW (Half Power Beam Width) for this frequency is 0°.35. The contours plotted represent the temperatures $T_{\min}$ and $T_{\max}$ from Table 1 and nine contours in between. The contours are plotted every 0.265 K, starting from the lowest temperature of 0.395 K and up to 0.66 K. The corresponding temperature scale is given (in K). Bottom: the 2720 MHz area map of Cygnus. The color figure can be viewed online.

show that it is applicable to almost all remnants. To confirm that our method works well, we also provide the area maps of Cygnus at the five frequencies (Figures 1–5) and some examples of the temperature profiles at 2720 MHz (Figure 6). In Figure 6 it should be noticed that the bottom panel shows only back-

[3]Available at the site `http://www.mpifr-bonn.mpg.de/survey.html`.

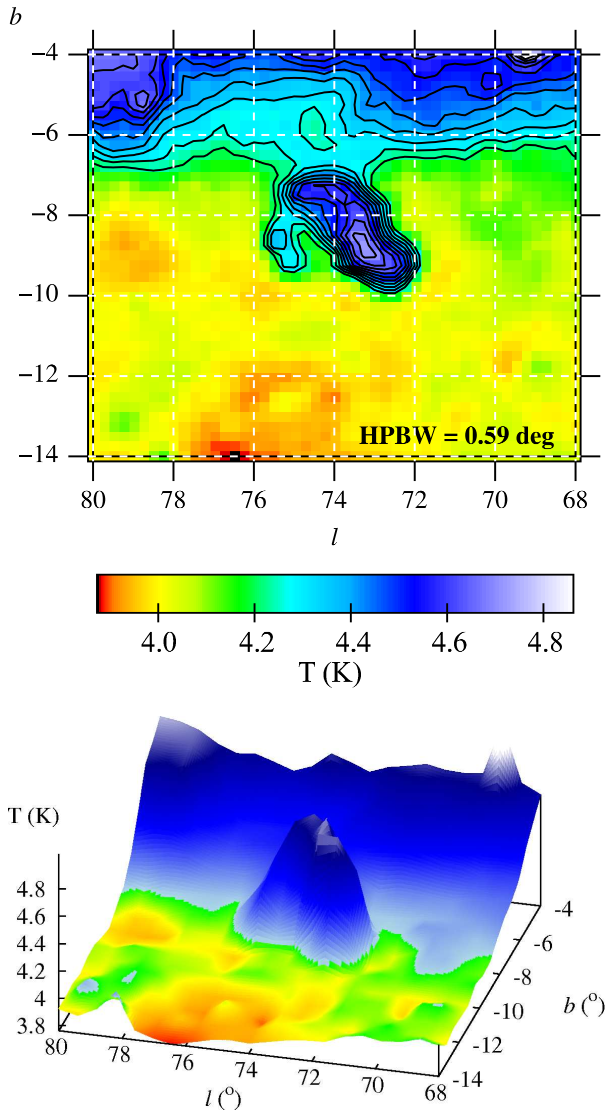

Fig. 2. The same as Figure 1, but for 1420 MHz. The HPBW for this frequency is 0°.59. The contours are plotted every 0.07 K, starting from the lowest temperature of 4.2 K and up to 4.9 K. The color figure can be viewed online.

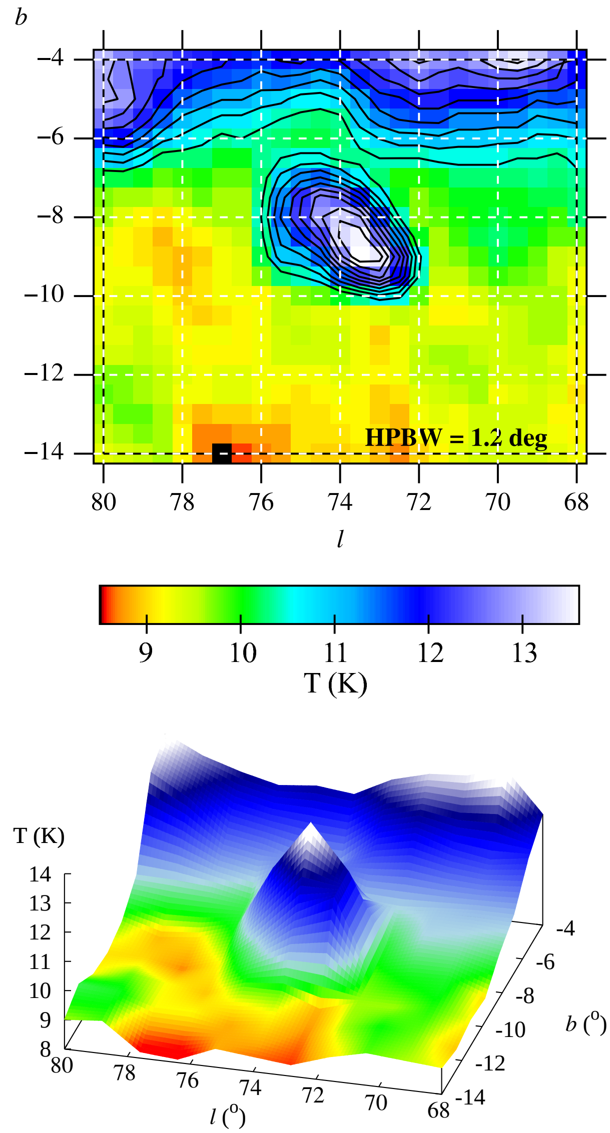

Fig. 3. The same as Figure 1, but for 820 MHz. The HPBW is 1°.2. The contours are plotted every 0.39 K, starting from the lowest temperature of 10.1 K and up to 14 K. The color figure can be viewed online.

ground radiation (not including the loop), where for $b = -10°$ the brightness temperature is not higher than 0.38 K. It is in agreement with the temperature intervals given in the first row of Table 1, where we posit 0.395 K for the minimum temperature of the loop with background, at 2720 MHz.

The mean temperatures and surface brightnesses of this radio loop are computed using data taken from radio-continuum surveys at 2720, 1420, 820, 408 and 34.5 MHz. We have subtracted the background radiation in order to derive the mean brightness temperature of the SNR alone. First, the temperature of the loop plus background was determined. For every bin in the survey we have some value for temperature $T_{\rm sum}$. We take all bins within the loop border and obtain the average temperature $<T_{\rm sum}>$ of the loop plus background. Then, the background alone near the loop was estimated. We determine the temperature of the background near the outer border of the loop (average value from all data near the outer border of the loop) and that is taken as the background temperature $T_{\rm back}$. And finally, the difference of these values is calculated to obtain the average temperature of the loop at

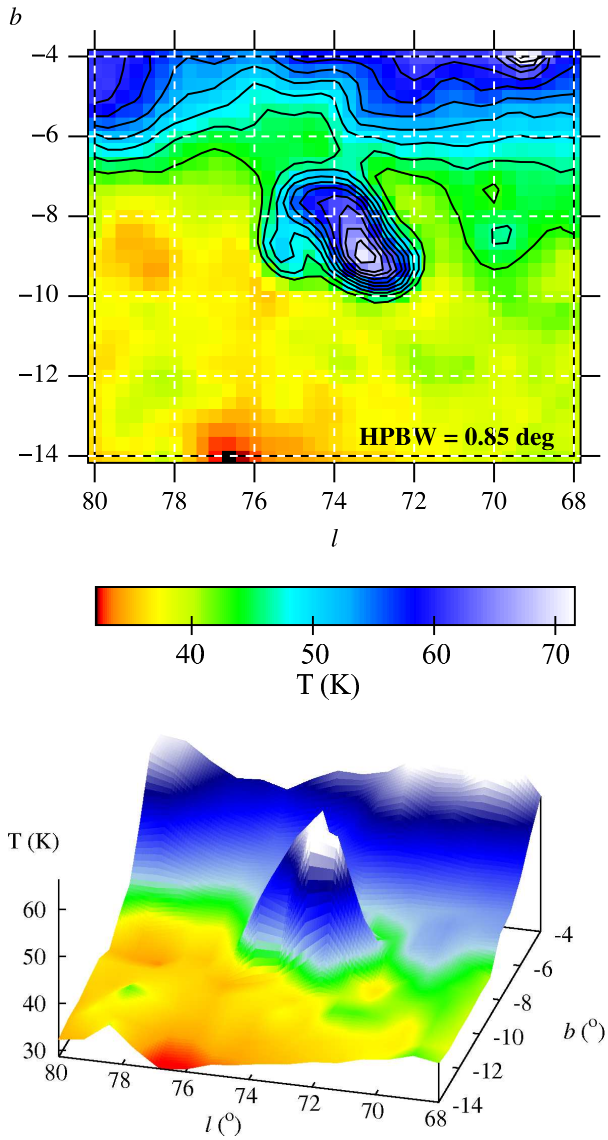

Fig. 4. The same as Figure 1, but for 408 MHz. The HPBW is 0°.85. The contours are plotted every 3.1 K, starting from the lowest temperature of 41 K and up to 72 K. The color figure can be viewed online.

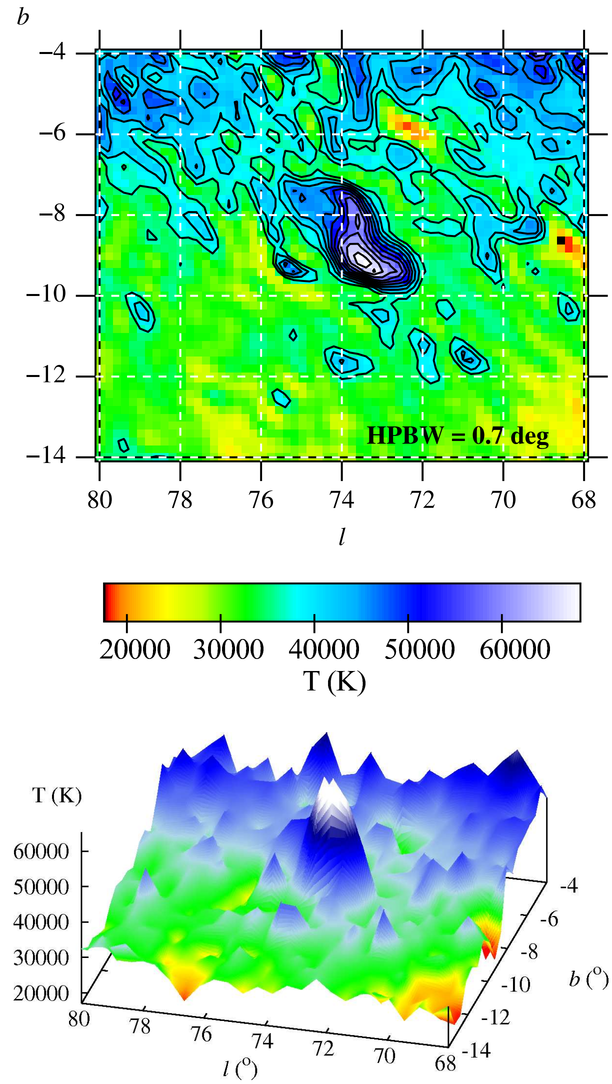

Fig. 5. The same as Figure 1, but for 34.5 MHz. The HPBW is 0°.7. The contours are plotted every 3550 K, starting from the lowest temperature of 34500 K and up to 70000 K. The color figure can be viewed online.

each frequency: average temperature of the loop is $<T_{\rm sum}> - T_{\rm back}$. The areas over which an average brightness temperature is determined at each of the five frequencies are taken to be as similar as possible within the limits of the measurement accuracy. $T_{\rm min}$ in Table 1 means the lower temperature limit between the background and the loop, and $T_{\rm max}$ means the upper temperature limit of the loop. So we used all measured values between $T_{\rm min}$ and $T_{\rm max}$, inside the corresponding regions of l and b, to calculate the brightness temperature of the loop including the background. The mean brightness temperature for the loop is found by subtracting the mean value of the background brightness temperature from the mean value of the brightness temperature over the area of the loop.

After deriving the mean brightness temperatures $T_{{\rm b},\nu}$, we have converted these values into surface brightness Σ_ν by:

$$\Sigma_\nu = \left(2k\nu^2/c^2\right) T_{{\rm b},\nu}\,, \qquad (1)$$

where k is the Boltzmann constant and c the speed of light. Results are given in Table 1.

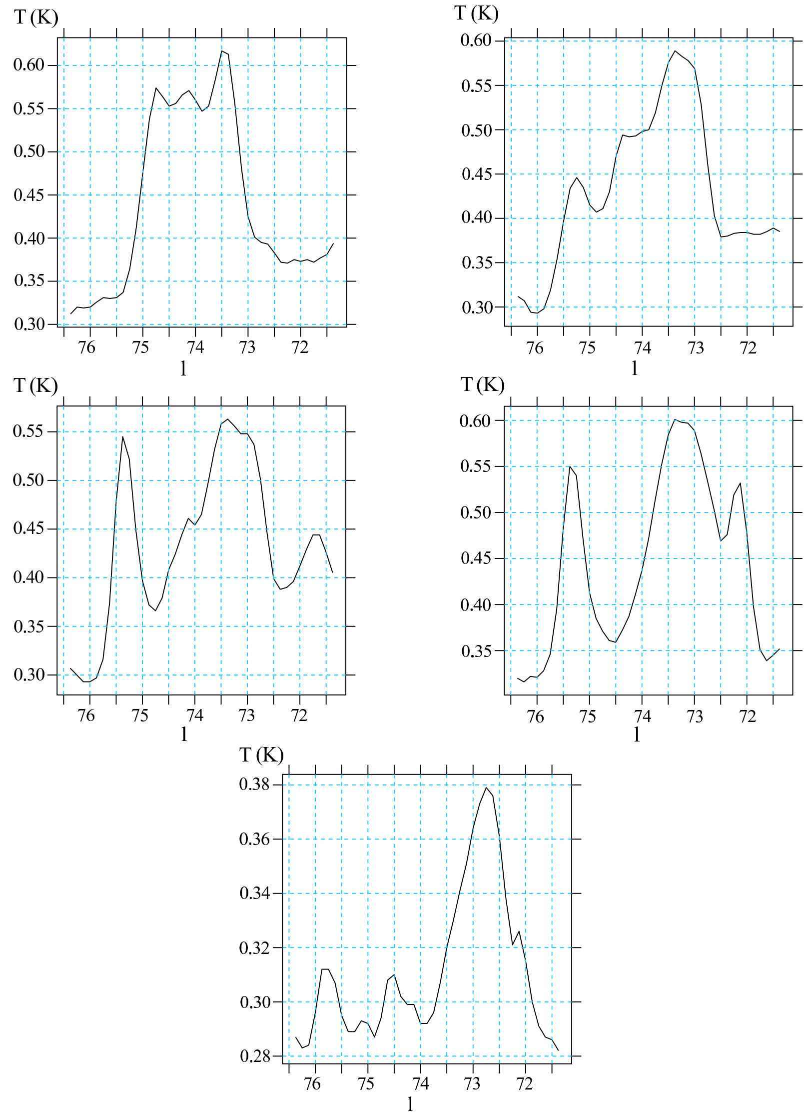

Fig. 6. Temperature profiles at 2720 MHz for Galactic longitude from 76°.5 to 71°.5 and for the following values of Galactic latitude: $b = -7^\circ.5$ (top left), $b = -8^\circ$ (top right), $b = -8^\circ.5$ (middle left), $b = -9^\circ$ (middle right) and $b = -10^\circ$ (bottom). Temperatures are given in K, and Galactic longitudes in degrees. Notice that the bottom figure shows the temperature profile at a latitude which lies outside (but close enough to) the loop, and from that profile we can see what is the highest temperature of the background at $b = -10^\circ$, at 2720 MHz (not of the loop with background).

3. RESULTS

The radio continuum maps are used for determining the area of the Cygnus loop and for deriving brightness temperatures over it. At each of the five frequencies, the areas are determined to be as similar as possible within the limits of measurement accuracy. There are still some differences between these areas and we think that the major causes of differing borders between the five frequencies are small random and systematic errors in the data. The surface brightnesses of SNRs must be above the sensitivity limit of the observations, and must be clearly distinguishable from the Galactic background emission (Green 1991). As it is very difficult to resolve the fainter parts of the loop from the background, they are not taken into account. For evaluation of the brightness temperatures over the area of the loop we had to take into account background radiation (see Webster 1974). Borders enclosing the spurs are defined to separate the spur and its background. For the method of calculation see also Borka (2007), Borka et al. (2008) and Borka Jovanović & Urošević

TABLE 1

TEMPERATURES AND BRIGHTNESSES OF THE CYGNUS RADIO LOOP AT 2720, 1420, 820, 408 AND 34.5 MHz

Frequency (MHz)	Temperature limits $T_{\rm min}$, $T_{\rm max}$ (K)	Temperature (K)	Brightness [10^{-22} W/(m^2 Hz Sr)]
2720	0.395, 0.66	0.160 ± 0.005	3.64 ± 0.12
1420	4.2, 4.9	0.49 ± 0.05	3.04 ± 0.30
820	10.1, 14.0	2.30 ± 0.20	4.75 ± 0.40
408	41, 72	15.3 ± 1.0	7.83 ± 0.50
34.5	34500, 70000	13960 ± 700	50.97 ± 2.56

TABLE 2

SPECTRAL INDICES FOR CYGNUS LOOP FROM $T-T$ PLOTS, BETWEEN 2720, 1420, 820, 408 AND 34.5 MHz

Frequency (MHz)	2720	1420	820	408	34.5
2720	⋯	1.52 ± 0.35	1.96 ± 0.53	2.35 ± 0.26	2.57 ± 0.23
1420	2.22 ± 0.76	⋯	2.27 ± 0.64	2.60 ± 0.28	2.67 ± 0.25
820	2.64 ± 0.61	3.10 ± 0.64	⋯	2.82 ± 0.31	2.82 ± 0.10
408	2.67 ± 0.26	2.79 ± 0.28	3.10 ± 0.31	⋯	2.78 ± 0.15
34.5	2.86 ± 0.23	2.95 ± 0.25	2.92 ± 0.10	2.94 ± 0.15	⋯

(2009b). As mentioned in these papers, if the value of $T_{\rm min}$ is changed by a small amount, the brightness contours become significantly different. If $T_{\rm min}$ is too small, the area of the spur becomes confused with the background and it becomes obvious that the border has been incorrectly chosen.

The results are given in Tables 1, 2 and 3. $T_{\rm min}$, given in the second column of Table 1, is the lower temperature limit, while $T_{\rm max}$ is the upper temperature of the loop and it is also the upper temperature limit (because there are no other superposed sources). These temperature limits enable us to distinguish the loop from the background. Then we derived the surface brightnesses using equation (1) for each frequency.

The values for the brightnesses in units of 10^{-22} W/ (m^2 Hz Sr) can be compared with results for the flux densities in Jy. The flux densities can be transformed into brightnesses or vice versa, taking into account that the frequencies have to be the same. Knowing the loop size Ω, the flux densities S_ν given in Jy can be transformed to brightnesses given in 10^{-22} W/(m^2 Hz Sr) by:

$$\Sigma_\nu = S_\nu \times 10^{-26}/\Omega\,. \qquad (2)$$

TABLE 3

BRIGHTNESS OF CYGNUS RADIO LOOP REDUCED TO 1000 MHz[a]

Frequency (MHz)	Brightness at 1000 MHz (10^{-22} W/(m^2 Hz Sr))
2720	7.05 ± 0.86
1420	3.84 ± 0.52
820	4.17 ± 0.29
408	4.33 ± 0.07
34.5	5.52 ± 1.40

[a]Using spectral index derived in this paper: $\beta_5 = 2.66 \pm 0.09$ (from the spectrum of all five frequencies 2720, 1420, 820, 408 and 34.5 MHz).

By use of the spectral indices, the brightnesses can be reduced to 1000 MHz according to the relation:

$$\Sigma_{1000} = \Sigma_\nu (1000/\nu)^{(2-\beta)}\,, \qquad (3)$$

where the temperature spectral index $\beta = \alpha + 2$, and α is the spectral index defined by $S_\nu \propto \nu^{-\alpha}$.

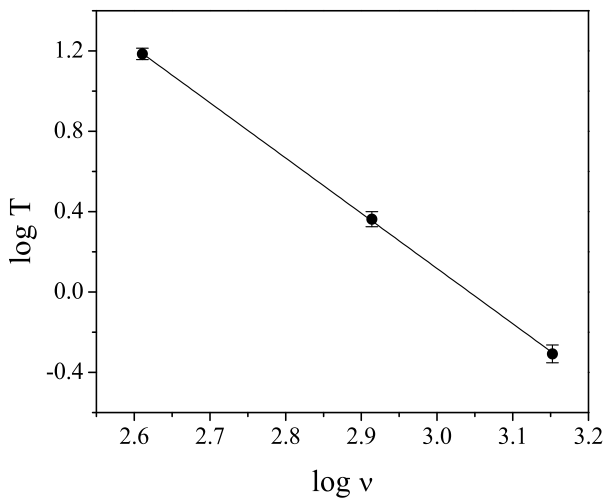

Fig. 7. Cygnus loop spectrum: temperature versus frequency, for three measurements (at 408, 820 and 1420 MHz).

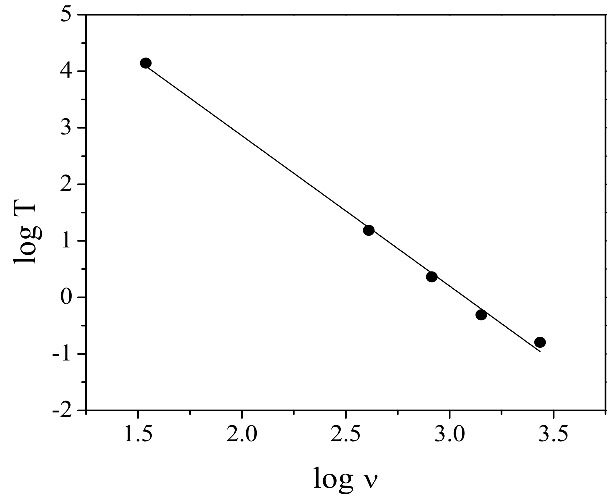

Fig. 8. Cygnus loop spectrum: temperature versus frequency, for five measurements (at 34.5, 408, 820, 1420 and 2720 MHz).

3.1. *Spectrum*

The spectrum was generated using mean temperatures at five different frequencies. The best-fit straight line spectrum enables the calculation of the spectral index as the negative value of the line's direction coefficient. In Figure 7 we show the spectrum for the three middle frequencies: 1420, 820 and 408 MHz because they are very well fitted with a straight line (see Figure 7). Frequencies 2720 and 34.5 MHz, lie on the very high and very low ends of the spectrum, as presented in Figure 8. If for the calculation of the spectral index we take only three frequencies 1420, 820 and 408 MHz, the result would be $\beta_3 = 2.76 \pm 0.03$. From a linear fit to all five frequencies 2720, 1420, 820, 408 and 34.5 MHz, we obtain $\beta_5 = 2.66 \pm 0.09$. It is a steeper spectral index in comparison to the average value for Galactic SNRs $\beta = 2.5$ (in Green's catalogue (Green 2009) the adopted value for the spectral index is not given because of its variability). The Cygnus loop is relatively old SNR. The shock wave has to be weak for evolved SNRs. The steeper spectral indices of SNRs should be expected for the smaller shock wave velocities. This is a result obtained from the diffuse particle acceleration theory (Bell 1978a,b). Additionally, the Cygnus loop probably expands in a low density environment. It looks like the large Galactic radio loops – evolved SNRs with steep spectral indices, immersed in a low density environment (see Borka 2007; Borka et al. 2008, and references therein).

The values we obtain, $\beta_3 = 2.76 \pm 0.03$ (from three frequencies), $\beta_5 = 2.66 \pm 0.09$ (from all five frequencies), are greater than 2.2 and confirm the nonthermal origin of the Cygnus loop emission. From Figure 8 it can be noticed that a linear fit is quite satisfactory. The value for the brightness temperature spectral index of the Cygnus loop is rather steep. This is at the high end of the spectral index distribution for SNRs as suggested in Clark & Caswell (1976).

3.2. $T - T$ *plot*

The measured data have different resolutions for different frequencies (see § 2.1), and therefore in order to obtain $T - T$ plots the data were retabulated: the higher resolution maps are convolved to the resolution of the lowest resolution map. In this way, we convolved data at 2720, 1420, 408 and 34.5 MHz to $0°.5 \times 0°.5$ resolution, which is the sampling rate of the 820 MHz survey. These retabulated data are presented in Figure 9 for the following frequencies: 2720 MHz (top left), 1420 MHz (top right), 820 MHz (middle left), 408 MHz (middle right) and 34.5 MHz (bottom). Then, for each frequency pair we used only the common points [with the same (l, b)] which belong to the loop area at both frequencies. In this way, we reduced the loop area to the same area for different frequencies. The obtained $T - T$ plots for five pairs of frequencies enabled the calculation of the spectral indices. We calculated two β values for each of these pairs: between 2720–1420, 2720–820, 2720–408, 2720–34.5, 1420–820, 1420–408, 1420–34.5, 820–408, 820–34.5 and 408–34.5 MHz. They are presented in Table 2.

For each of the ten frequency pairs, by interchanging the dependent and independent variables we obtained two β values for each pair and the mean value of these results is adopted as the radio spectral index, as suggested in Uyaniker et al. (2004). Regarding only three frequencies (because their spectrum lies on straight line, see Figure 7) 1420, 820 and 408 MHz, the average value of spectral index from $T-T$ is $<\beta_{TT}>_3 = 2.78 \pm 0.41$. Taking into account all five frequencies, we get $<\beta_{TT}>_5 = 2.63 \pm 0.30$. It can be noticed that, as expected, this value agrees well with the corresponding value obtained from the spectrum (see Uyaniker et al. 2004).

Then we calculated the mean value of the spectral index: regarding spectrum and $T-T$ graphs. Between 1420, 820 and 408 MHz we obtained $<\beta>_3 = 2.77 \pm 0.22$, and between 2720, 1420, 820, 408 and 34.5 MHz we obtained $<\beta>_5 = 2.64 \pm 0.20$.

4. DISCUSSION

The spectral index variations with position of more spatial features within the Cygnus loop can be found in the paper by Leahy (1999). He studied radio spectral indices by the $T-T$ plot method between 2695, 1420 and 408 MHz and found that the bright radio filaments all show negative curvature (steeper at higher frequency), and that regions dominated by diffuse emission show positive curvature (flatter at higher frequency).

It can be noticed that the mean value of spectral index for the Cygnus loop is a little higher then the corresponding value obtained from the literature (see Uyaniker et al. 2004 or Leahy & Rogers 1998). The reason for this is the different areas used for data of the Cygnus loop in these papers. In both papers they used square areas (see page 917 from Uyaniker et al. 2004, and page 786 from Leahy & Roger 1998). In these square areas they took into account parts of the Cygnus loop and parts of the background radiation near the loop (these parts we do not take into account). We take in account only higher intensity regions from these areas (see Figures 1–5).

In order to compare our values for the brightnesses with results for the fluxes given in other papers, we transform their calculated fluxes into brightnesses at 1000 MHz. Knowing the loop size Ω we reduce the flux densities given in Jy to brightnesses given in $10^{-22}\,\mathrm{W/(m^2\ Hz\ Sr)}$ by means of equation (2) and then, using the spectral indices, the brightnesses are extrapolated to 1000 MHz according to relation (3).

In our previous paper (Borka Jovanović & Urošević 2009a) we transformed the flux densities for the Cygnus Loop given in Roger et al. (1999) at 22 MHz ($S_\nu = 1378$ Jy) and Reich et al. (2003) at 863 MHz ($S_\nu = 184$ Jy) into Σ_{1000} using the loop size $\Omega = 240' \times 170'$ from Reich et al. (2003) and the spectral index $\beta = 2.49$ from Trushkin (2002). We obtained that the values from Borka Jovanović & Urošević (2009a) agree with previous data. In this paper, we use our derived value for the spectral index $\beta_5 = 2.66 \pm 0.09$, and obtain even better agreement. From the flux densities given in the paper mentioned, we calculated the following values for radiation intensities: $\Sigma_{1000} = 3.22 \times 10^{-22}\,\mathrm{W/(m^2\ Hz\ Sr)}$ from the flux given in Roger et al. (1999) and $\Sigma_{1000} = 4.84 \times 10^{-22}\,\mathrm{W/(m^2\ Hz\ Sr)}$ from the flux given in Reich et al. (2003).

Using our calculated β_5 and applying relation (3) to our calculated values of Σ_ν at 2720, 1420, 820, 408 and 34.5 MHz, for Σ_{1000} we obtain the values given in Table 3. Absolute errors for brightnesses at 1000 MHz are calculated in this way: $\Delta\Sigma_{1000} = (\Sigma_{1000}/\Sigma_{\nu 1})\,(\Delta\Sigma_{\nu 1} + \Sigma_{\nu 1} \cdot \ln(\nu_1/1000) \cdot \Delta\beta)$, where ν_1 takes values 2720, 1420, 820, 408 and 34.5 MHz.

Information about variations of the brightness and the spectrum over the radio image is presented by Leahy & Roger (1998) and by Uyaniker et al. (2002). The average values reduce the information imprinted in variations of brightness and spectrum over the radio image but give us other interesting information, like the explosion energy, the surface brightness and the distance to the Cygnus radio loop.

With regard to the loop borders in Figures 1–5, we derived the loop area at each frequency, as well as the corresponding angular radii (see Table 4). An angular radius is obtained in this way: our derived loop area, when approximated with a circle of the same area, gives the possibility of determining the angular radius as $\theta = \sqrt{\Omega/\pi}$. These areas can be compared to the areas calculated by other authors, e.g., $9(^\circ)^2.80$ at 1420 MHz (Leahy 2002) and $11(^\circ)^2.33$ at 863 MHz (Reich et al. 2003). When their areas are recalculated into angular radii in the way we described, the result are: $1^\circ.77$ at 1420 MHz (Leahy 2002) and $1^\circ.90$ at 863 MHz (Reich et al. 2003). It can be noticed that we obtained somewhat smaller values, but it has to be taken into account that other authors estimated only the rectangular map size while we estimated the loop size (inside its contour borders) exactly.

The relation between surface brightness (Σ) and diameter (D) for supernova remnants (SNRs) –so-called the $\Sigma - D$ relation– is appropriate for the description of the radio brightness evolution of these sources. The empirical relations should be used

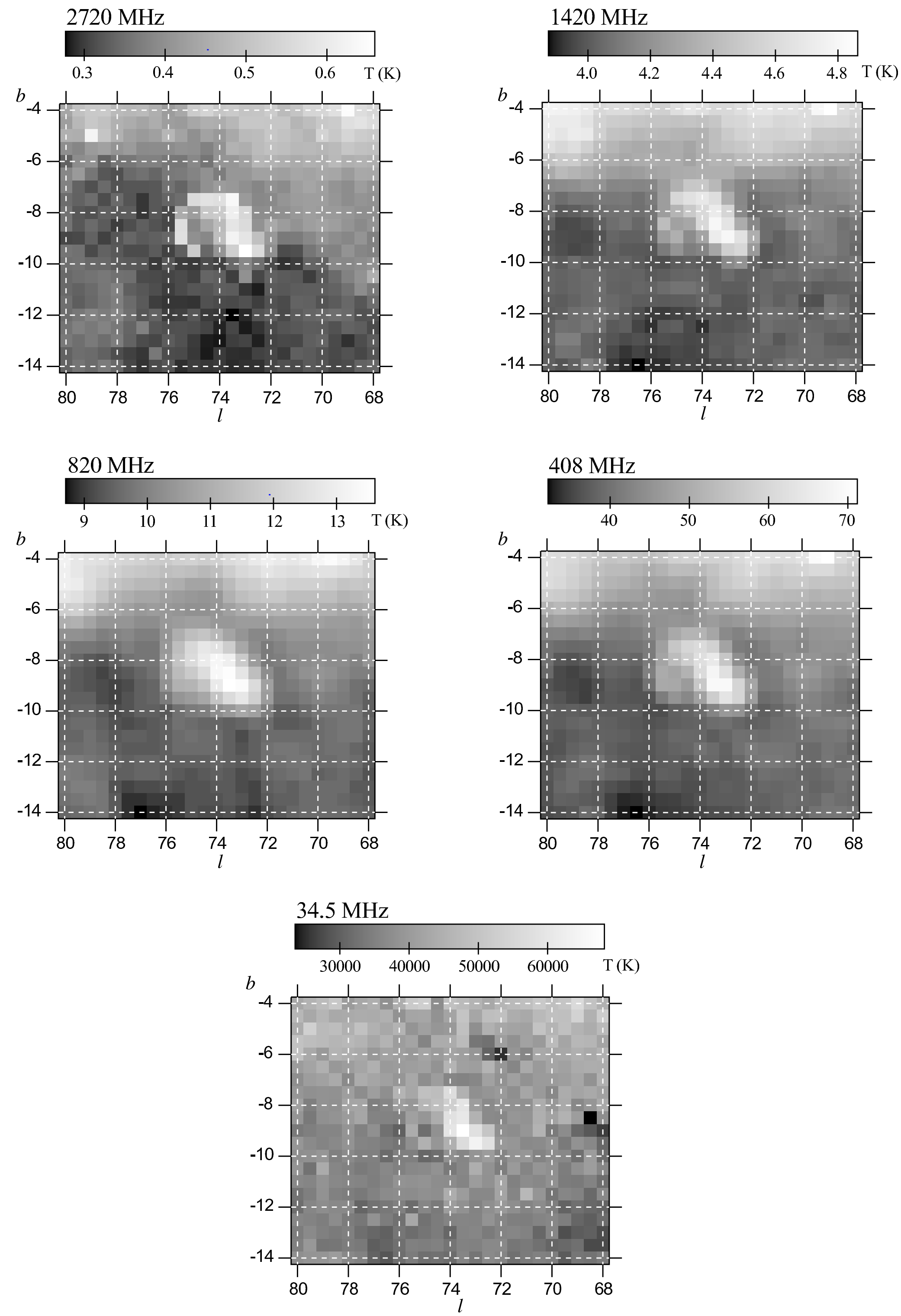

Fig. 9. The data retabulated to $0^\circ.5 \times 0^\circ.5$ resolution, for the following frequencies: 2720 MHz (top left), 1420 MHz (top right), 820 MHz (middle left), 408 MHz (middle right) and 34.5 MHz (bottom). The HPBWs for these frequencies are $0^\circ.35$, $0^\circ.59$, $1^\circ.2$, $0^\circ.85$ and $0^\circ.7$, respectively. The gray scales of temperatures are also given.

TABLE 4

THE CYGNUS LOOP AREAS Ω AND ANGULAR RADII θ AT THE FIVE FREQUENCIES

Frequency (MHz)	Ω $[(^\circ)^2]$	θ $(^\circ)$
2720	7.52	1.547
1420	8.64	1.658
820	9.46	1.735
408	9.88	1.773
34.5	8.44	1.639

with caution because of the limited usefulness due to selection effects (see Green 2009; Urošević 2010, and references therein). The updated theoretical relations were derived by Duric & Seaquist (1986), based on the Bell (1978a,b) diffuse shock particle acceleration theory, and by Berezhko & Völk (2004) based on the non-linear kinetic theory of the diffuse shock acceleration mechanism. The $\Sigma - D$ diagram at 1 GHz with the theoretically derived evolutionary tracks taken from Berezhko & Völk (2004) and with our value for the Cygnus loop superposed, is shown in Figure 10. To superpose the Cygnus position, we used the following results of our calculations: the mean value of the brightnesses at 1 GHz and the diameter, calculated as $D = 2r\sin\bar{\theta}$, where $\bar{\theta} = 1^\circ.67$ is the mean angular radius for all five frequencies. The distance $r = 0.44$ kpc is taken from Green's (2009) catalogue of SNRs. So we added this point to the diagram: $(D, \Sigma) = (25.7$ pc, 4.98×10^{-22} W/(m^2 Hz Sr)). From its position in this diagram it can be concluded that the Cygnus loop evolves in the low density environment and the initial energy of the supernova (SN) explosion was relatively low (see Figure 10).

4.1. *Flux density spectrum*

On the basis of the values for brightnesses given in the fourth column of Table 1 and our calculated values for the loop size Ω (Table 4), we derived flux values in Jy. The calculated flux densities are given in Table 5. As the Cygnus loop is well studied SNR, it is possible to perform a multi-frequency spectral study. In Figure 11 we present a summary of some results obtained from other papers and from our study. Our results are labeled with asterisks. In this figure, we have seventeen results for the flux density values S_ν of Cygnus loop derived in several papers (values are given in Table 3 of Uyaniker et al. (2004) and five results from our paper.

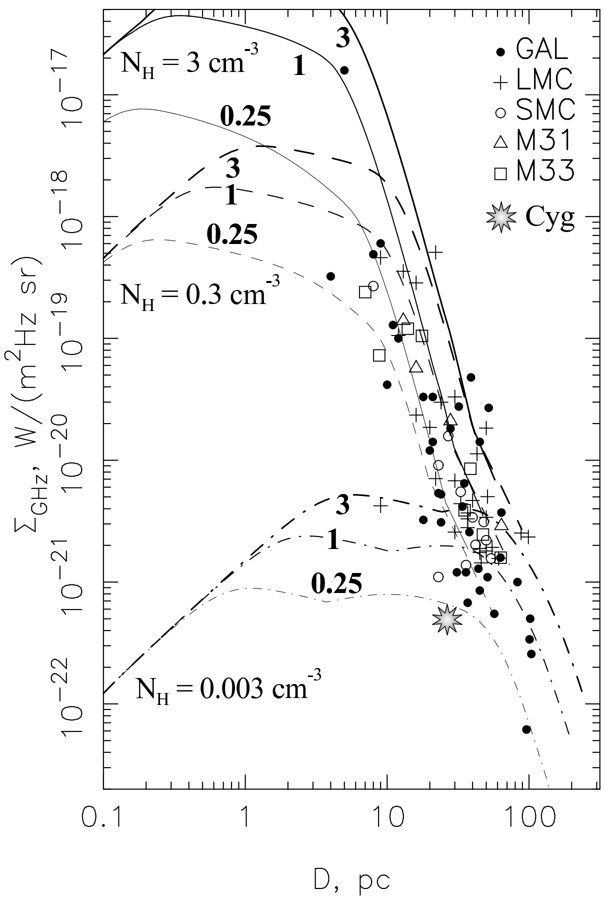

Fig. 10. The surface brightness versus diameter diagram from Berezhko & Völk (2004), with the value for Cygnus loop added. Three different densities for the interstellar matter (ISM) ($N_{\rm H} = 3$, 0.3 and 0.003 cm^{-3}) are presented, plus three values for the (SN) explosion energy ($E_{\rm SN} = 0.25$, 1 and 3×10^{51} erg).

It can be seen from Figure 11 that our added flux values fit very well among other fluxes, which shows the correctness of our method, and also that we determined the loop area and its brightness well.

TABLE 5

FLUX DENSITIES (Jy) THAT WE CALCULATED AT THE FIVE FREQUENCIES

Frequency (MHz)	Flux density (Jy)
2720	83.37±2.60
1420	80.05±8.13
820	139.35±12.10
408	235.44±15.36
34.5	1309.04±65.65

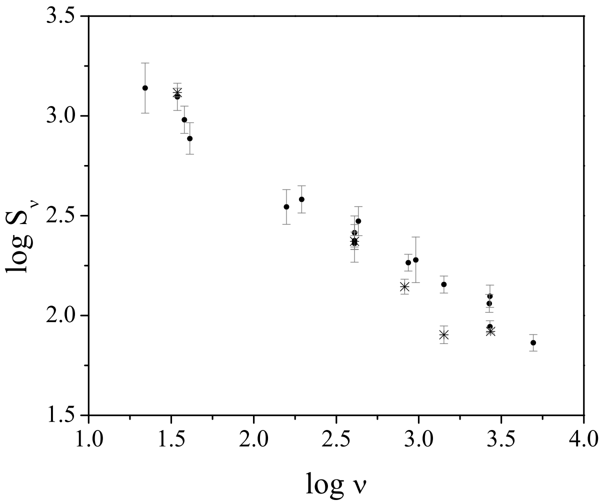

Fig. 11. Spectrum of Cygnus Loop: flux versus frequency for additional different frequencies, obtained from all available flux density values (values are given in Table 3 in Uyaniker et al. 2004) and from values calculated in this paper. We identify our values by asterisks.

5. CONCLUSIONS

The main result is to use a method for determining the brightness temperature given in Borka (2007) which is developed for large radio loops, and to show here that this method is applicable for much smaller loops, e.g., the Cygnus loop. We check the method by applying it to the Cygnus radio loop over a wide range of frequencies. It is in good agreement with the method of $T-T$ graphs and with results obtained with other methods. This method is quite simple because we use a brightness temperature isoline to define the border of the Cygnus loop. Other authors are using different square or rectangular areas to determine the area of the loop and to calculate spectral indices, brightness temperatures and the flux density of the loop (Uyaniker et al. 2004, page 917, and Leahy & Roger 1998, page 786). Also, we calculate the flux for the Cygnus loop and compare our results with those of other authors in different ranges of frequencies. We show that our results are in good agrement with other work.

We estimate the temperatures and brightness of the Cygnus loop SNR on the basis of observations of the continuum radio emission at the frequencies: 2720, 1420, 820, 408 and 34.5 MHz (this paper and Borka Jovanović & Urošević (2009a). The sensitivity of the brightness temperatures are: 5 mK for 2720 MHz, 50 mK for 1420 MHz, 0.2 K for 820 MHz, 1.0 K for 408 MHz and about 700 K T_b for 34.5 MHz. At a frequency of 2720 MHz the measurements are the most precise (they have the smallest relative errors) so positions of the brightness temperature contours of the loop are the most realistic for this frequency.

The borders between the five frequencies are somewhat different for this SNR, probably due to small, random and systematic errors in the calibrated data. Also, we suppose that there are uncertainties of about ($2\times\Delta T$) 10 mK for 2720 MHz, 100 mK for 1420 MHz, 0.4 K for 820 MHz, 2.0 K for 408 MHz and about 1400 K T_b for 34.5 MHz, in the border due to measurement errors, and there is a tiny difference in the absorption of radio emission in the interstellar medium at different wavelengths (Pacholczyk 1970).

We determine the average brightness temperature for the Cygnus radio loop region, after subtraction of a background level. Our values (when all reduced to 1000 MHz for comparison) are in good agreement with the earlier results. We present the radio continuum spectrum of the Cygnus loop using average brightness temperatures at five different frequencies. As can be seen from Figures 7 and 8, the linear fit provides a reliable spectral index. We present the $T-T$ plots which also enable the calculation of spectral index.

Also, from our results it can be concluded that the Cygnus loop evolves in a low density environment and that the initial energy of SN explosion was relatively low. This can be read off after superposing the position of this loop onto a theoretical $\Sigma-D$ diagram from Berezhko & Völk (2004), which was derived from non-linear kinetic theory of diffuse shock acceleration mechanism.

We show that our method for defining a loop border and for determining the values of temperature and brightness, which was developeded for main Galactic loops I-VI, could be applicable to all SNRs.

The authors are grateful to the referee whose suggestions substantially improved the paper. This research is supported by the Ministry of Science of the Republic of Serbia through project No. 176005.

REFERENCES

Aschenbach, B., & Leahy, D. A. 1999, A&A, 341, 602

Bell, A. R. 1978a, MNRAS, 182, 147

________. 1978b, MNRAS, 182, 443

Berezhko, E. G., & Völk, H. J. 2004, A&A, 427, 525

Berkhuijsen, E. M. 1972, A&AS, 5, 263

Borka, V. 2007, MNRAS, 376, 634

Borka, V., Milogradov-Turin, J., & Urošević, D. 2008, Astron. Nachr., 329, 397

Borka Jovanović, V., & Urošević, D. 2009a, Publ. Astron. Obs. Belgrade, 86, 101
__________. 2009b, Astron. Nachr., 330, 741
Clark, D. H., & Caswell, J. L. 1976, MNRAS, 174, 267
Dickel, J. R., & Willis, A. G. 1980, A&A, 85, 55
Duric, N., & Seaquist, E. R. 1986, ApJ, 301, 308
Dwarakanath, K. S., & Udaya Shankar, N. 1990, J. Astrophys. Astron., 11, 323
Green, D. A. 1984, MNRAS, 211, 433
__________. 1991, PASP, 103, 209
__________. 2004, Bull. Astron. Soc. India, 32, 335
__________. 2006, A Catalogue of Galactic Supernova Remnants (2006 April version) (Cambridge: Cavendish Laboratory)
__________. 2009, Bull. Astron. Soc. India, 37, 45
Haslam, C. G. T., Salter, C. J., Stoffel, H., & Wilson, W. E. 1982, A&AS, 47, 1
Keen, N. J., Wilson, W. E., Haslam, C. G. T., Graham, D. A., & Thomasson, P. 1973, A&A, 28, 197
Kundu, M. R., & Becker, R. H. 1972, AJ, 77, 459
Leahy, D. A. 1999, ASP Conf. Ser. 168, New Perspectives on the Interstellar Medium, ed. A. R. Taylor, T. L. Landecker, & G. Joncas (San Francisco: ASP), 437
__________. 2002, AJ, 123, 2689
Leahy, D. A., & Roger, R. S. 1998, ApJ, 505, 784
Leahy, D. A., Roger, R. S., & Ballantyne, D. 1997, AJ, 114, 2081
McKee, C. F., & Ostriker, J. P. 1977, ApJ, 218, 148
Pacholczyk, A. G. 1970, Radio Astrophysics. Nonthermal Processes in Galactic and Extragalactic Sources (San Francisco: Freeman)
Patnaude, D. J., Fesen, R. A., Raymond, J. C., Levenson, N. A., Graham, J. R., & Wallace, D. J. 2002, AJ, 124, 2118
Reich, P., & Reich, W. 1986 A&AS, 63, 205
Reich, W., Zhang, X., & Fürst, E. 2003, A&A, 408, 961
Reif, K., Reich, W., Steffen, P., Müller, P., & Weiland, H. 1987, Mitt. Astron. Ges., 70, 419
Roger, R. S., Costain, C. H., Landecker, T. L., & Swerdlyk, C. M. 1999, A&AS, 137, 7
Salter, C. J. 1983, Bull. Astron. Soc. India, 11, 1
Sun, X. H., Reich, W., Han, J. L., Reich, P., & Wielebinski, R. 2006, A&A, 447, 937
Trushkin, S. A. 2002, CATS Database-Astrophysical CATalogs Support System, SNRs Spectra Request Form, `http://www.sao.ru/cats/snr_spectra.html`
Urošević, D., Vukotić, B, Arbutina, B., & Sarevska, M. 2010, ApJ, 719, 950
Uyaniker, B., Reich, W., Yar, A., & Fürst, E. 2004, A&A, 426, 909
Uyaniker, B., Reich, W., Yar, A., Kothes, R., & Fürst, E. 2002, A&A, 389, L61
Webster, A. S. 1974, MNRAS, 166, 355

V. Borka Jovanović: Atomic Physics Laboratory (040), Vinča Institute of Nuclear Sciences, University of Belgrade, P.O. Box 522, 11001 Belgrade, Serbia (vborka@vinca.rs)
D. Urošević: Department of Astronomy, Faculty of Mathematics, University of Belgrade, Studentski trg 16, 11000 Belgrade, Serbia (dejanu@matf.bg.ac.rs).